

# A Practical Analysis: Understanding Phase Noise Modelling in Time and Frequency Domain for Phase-Locked Loops

Carl Collmann, Bitan Banerjee, Ahmad Nimr, Gerhard Fettweis

Vodafone Chair Mobile Communications Systems, Technische Universität Dresden, Germany  
{carl.collmann, bitan.banerjee, ahmad.nimr, gerhard.fettweis}@tu-dresden.de

**Abstract**—In multiple-input multiple-output (MIMO) systems, the presence of phase noise is a significant factor that can degrade performance. For MIMO testbeds build from software-defined radio (SDR) devices, phase noise cannot be ignored, particular in applications that require phase synchronization. This is especially relevant in MIMO systems that employ digital beamforming, where precise phase alignment is crucial. Accordingly, accurate phase noise modelling of SDR devices is essential. However, the information provided in data sheets for different SDR models varies widely and is often insufficient for comprehensive characterization of their phase noise performance. While numerical simulations of phase-locked loop (PLL) phase noise behavior are documented in the literature, there is a lack of extensive measurements supported by appropriate system modelling. In this work, we present a practical phase noise modeling methodology applied to an SDR from the universal software radio peripheral (USRP) X310 series. Based on measurement data, we derive estimates of key PLL performance indicators such as cycle-to-cycle jitter, oscillator constants, and PLL bandwidth. Furthermore, we propose a parametric model for the phase noise power spectral density (PSD) of the PLL circuit and provide corresponding parameter estimates. This model can be used for further investigation into the impact of phase noise on MIMO system performance implemented by similar SDR devices.

**Index Terms**—phase noise, SDR, phase-locked loop

## I. INTRODUCTION

The upcoming sixth generation (6G) of mobile communication networks aims to achieve improved data rates, low latency, and highly reliable connections [1]. To meet these specifications, increased bandwidth at higher carrier frequency is adopted. However, at higher frequencies and bandwidths, the effect of hardware impairments such as phase noise, becomes significantly more pronounced and cannot be ignored. Therefore, it is essential to develop rigorous models and thorough explanations of phase noise effect.

In joint communications and sensing systems (JC&S), the common phase error (CPE), to which phase noise contributes, can severely influence the system performance. The phase noise causes intercarrier interference (ICI), which reduces the efficiency of data transmission. Additionally, the sensing accuracy can be adversely affected by the presence of phase noise [2]. Similarly, in multiple-input multiple-output (MIMO) systems, phase noise can degrade spatial multiplexing gains because it deteriorates the coherent combination of signals [3].

A reliable model of phase noise is required to enable the design of algorithms capable of mitigating its impairing ef-

fects. While the topic of phase noise in frequency-synthesizing circuits has received significant attention, many existing works face limitations. For instance, in [4] and [5], a rigorous unifying theory of phase noise analysis is introduced, which has gained widespread acceptance. However, this theory is presented without explicit validation through measurements. Subsequent works, such as [6], build upon this theory and improve its accessibility but still fail to establish strong links between theory and empirical observations. In [7], a method for phase tracking using a Kalman filter is investigated and experimentally validated with software-defined radio (SDR). However, the authors investigate primarily the Allan deviation rather than explicitly addressing the phase noise process. Other works, such as [8], primarily focus on presenting phase noise measurements in different scenarios but provide limited corresponding modelling of the phase noise.

The 3GPP standard also offers a phase noise model [9]. For a specific phase-locked loop (PLL), measurements are first performed, and then the parameters of a digital filter are fitted to these measurements to generate an empirical phase noise model. However, estimators for these parameters are not provided, and the model is limited to the phase noise spectrum. Consequently, the time-domain behavior of the phase noise process, particularly its non-stationary characteristics, can not be extrapolated. Furthermore, the dynamics of the PLL circuit are not modeled. While this kind of analysis can provide useful abstraction, more dedicated approaches are known [4] and might be more applicable, depending on the desired use-case of the model.

## A. Contribution

The contributions of this paper are as follows

- A simplified parametric phase noise spectrum model is derived by modelling the phase noise process and PLL dynamics in the time domain.
- The phase noise spectrum for common SDR devices is measured, and the impact of various radio frequency (RF) frontend daughterboards and frequencies is analyzed.
- Estimators for the parameters of the derived phase noise model are provided, bridging the established theoretical model with empirical observation.

## B. Organization

The rest of the paper is organized as follows: In section II, a general system model for phase noise is described. Next, a model for a free-running voltage-controlled oscillator (VCO) in the time domain and its corresponding phase noise spectrum is derived in section III. This model is then expanded to a PLL circuit in section IV. A model of stochastic differential equations in the time domain is presented along with the corresponding derivations to obtain the phase noise spectrum. In section V, the measurement setup is introduced. An overview of the recorded datasets are provided, highlighting the distinction of the phase noise spectrum of different daughterboard models for the universal software radio peripheral (USRP)'s evaluated. In section VI, the previously derived model is expanded to match the characteristics of the device under test (DUT). Estimators for deriving system parameters are introduced, and the corresponding estimates are presented for two USRP daughterboard models. Finally, the paper is concluded in section VII.

## II. OVERVIEW OF PHASE NOISE

Phase noise generally refers to a random change in the phase of a signal. In the time domain, this random change is commonly referred to as jitter. IEEE [10] defines phase noise as the single-sideband phase noise spectrum of the power spectral density (PSD) of phase fluctuations. Phase noise is given as  $\mathcal{L}(f_{\text{offs}})$  in dBc/Hz (power relative to carrier) at offset  $f_{\text{offs}}$  relative to carrier frequency. While an ideal oscillator produces a signal of a constant frequency, real oscillators are not stable in frequency. This fluctuation in frequency is linked to a corresponding time interval error (TIE) or fluctuation in the time domain. To characterize this fluctuation, we use a stochastic time shift  $\alpha(t)$ . The time shift can be translated into a phase shift  $\phi(t) = 2\pi f_0 \alpha(t)$  for a given oscillator frequency.

In the following, the effect of a stationary phase noise process in the time domain for a free running oscillator is analyzed and properties of a non-stationary phase noise process are described. This model is extended in following sections, where at first the impact of non-stationary phase noise processes on free running oscillators is explored. Finally, the model is extended to the entire PLL circuit. Each model covers time domain signals of phase noise processes and the corresponding frequency domain representations. The presented derivations follow those established in previous research [4]–[6].

### A. PSD of Oscillators Affected by a Stationary Noise Process

The output signal of an ideal oscillators first harmonic can be described as

$$x_0(t) = A x_{\text{CLK}}(2\pi f_0 t + \phi_0). \quad (1)$$

The amplitude of the oscillator signal  $A$  is assumed to be constant. The default phase shift of the oscillator signal is called  $\phi_0$ . The term  $x_{\text{CLK}}$  represents a generic oscillator clock function such as sine or square wave. In the following,  $\cos$  is used as oscillator clock function, with default frequency

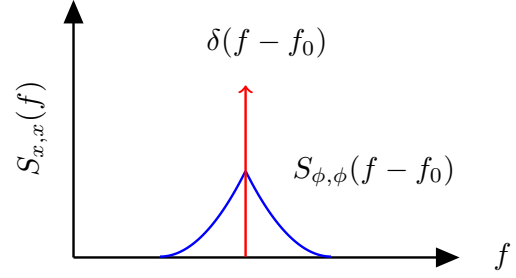


Fig. 1. PSD of a generic noisy oscillator with phase noise spectrum  $S_{\phi,\phi}$

$f_0$ . The output signal of a disturbed oscillator, applying the mentioned simplifications, is

$$x_{\text{PN}}(t) = \cos(2\pi f_0 t + \phi(t)) = \Re \left\{ e^{j(\omega_0 t + \phi(t))} \right\}. \quad (2)$$

The time dependent phase shift process  $\phi(t)$  representing the phase noise, can also be modeled by a time shift process  $\alpha(t) = \phi(t)/2\pi f_0$ . In this section,  $\phi(t)$  is assumed to be a stationary so that the PSD can be computed. To simplify the following derivation, the complex representation of the oscillator signal is used

$$x_{\text{PN}} = e^{j(\omega_0 t + \phi(t))} = e^{j(\omega_0 t + \omega_0 \alpha(t))}. \quad (3)$$

Assuming that the term  $\phi(t)$  is sufficiently small, a Taylor series approximation is applied

$$x_{\text{PN}} \approx e^{j\omega_0 t} (1 + j\phi(t)). \quad (4)$$

Next, the autocorrelation function (ACF) is calculated, assuming that the ACF of the noise term  $R_{\phi,\phi}(\tau)$  is known. Furthermore it is assumed that the oscillator signal is uncorrelated with the zero mean noise process so that the corresponding cross terms in the expectation vanish,

$$\begin{aligned} R_{x,x}(t, t + \tau) &= \mathbb{E} [x_{\text{PN}}(t) x_{\text{PN}}^*(t + \tau)] \\ &= e^{-j\omega_0 \tau} (1 + R_{\phi,\phi}(\tau)) \end{aligned} \quad (5)$$

To obtain the PSD, the Fourier transform of the ACF has to be calculated. In this context  $S_{\phi,\phi}(f) = \mathfrak{F}_\tau \{ R_{\phi,\phi}(\tau) \}$  denotes the phase noise PSD. Then the output spectrum of a generic noisy oscillator is given as

$$\begin{aligned} S_{x,x}(f) &= \mathfrak{F}_\tau \{ R_{x,x}(t, t + \tau) \} \\ &= \delta(f - f_0) + S_{\phi,\phi}(f - f_0) \end{aligned} \quad (6)$$

It can be seen that the PSD consists of a Dirac pulse at the oscillators frequency and the noise spectrum component that centered around the oscillator frequency  $f_0$  (as illustrated in Fig. 1)

### B. Wiener Process

In established research, it is common practice to model the phase noise as a Wiener process [4]. A Wiener process is a non-stationary stochastic process characterized by independent normally distributed increments. The Wiener process  $W(t)$

can be characterized as the integral over a zero mean, white Gaussian process  $\xi(t)$  of unit variance

$$W(t) = \int_0^t \xi(t') dt' = \int_0^{W(t)} dW(t'). \quad (7)$$

Note that a differential step of a Wiener process is defined as

$$dW(t) \equiv W(t + dt) - W(t) = \xi(t)dt. \quad (8)$$

It is assumed that the stochastic time shift  $\alpha(t) = \sqrt{c_{VCO}}W(t)$  affecting a free running oscillator can be modelled as a Wiener process. In this case, the Wiener process is scaled with the oscillator specific constant  $c_{VCO}$ . Then, the following properties hold for the process of stochastic time shifts [11], [12, p. 445 ff.]:

1.  $\alpha(t)$  is zero mean and not stationary

$$\mathbb{E}[\alpha(t)] = 0.$$

2. The variance of the process grows linear with time  $t$

$$\sigma_\alpha^2(t) = \mathbb{E}[\alpha(t)^2] = c_{VCO}t. \quad (9)$$

3. At time instance  $\tau$ , the random variable  $\alpha(t = \tau)$  is gauss-distributed. Its density function is given as

$$f_\alpha(z, t) = \frac{1}{\sqrt{2\pi c_{VCO}t}} e^{-\frac{z^2}{2c_{VCO}t}}.$$

4. increments of the process  $\alpha(t)$  are independent

$$\mathbb{E}[(\alpha(\tau_1) - \alpha(\tau_0))(\alpha(\tau_0))] = 0, \text{ for } \tau_0 < \tau_1.$$

5. The autocorrelation function for the process  $\alpha(t)$  is given as (c.f. [4, Corollary 7.1])

$$R_{\alpha,\alpha}(t, t + \tau) = c_{VCO}t, \text{ for } \tau > 0. \quad (10)$$

### III. FREE RUNNING OSCILLATOR

This section describes the modeling of a generic free-running oscillator affected by a Wiener phase noise. The model considers a VCO subjected to white Gaussian noise at its control voltage. Key findings from prior analyses [4] are:

1. The process  $\alpha(t)$  of random time shifts affecting the ideal free running oscillator can asymptotically, i.e.,  $t \rightarrow \infty$ , be described as a Wiener-process and is Gaussian distributed.
2. The output of a noisy oscillator is asymptotically stationary. Its corresponding PSD consists of Lorentzian spectra, symmetrically centered around the harmonics of an undisturbed oscillator.
3. A scalar constant  $c_{VCO}$  is sufficient to characterize the process  $\alpha(t)$  and the corresponding PSD of a noisy oscillator.

#### A. Voltage Controlled Oscillator Model

Analyzing the case of a free-running VCO, further assumptions are:

4. The oscillator is affected by independent white noise processes that can be combined to a single white Gaussian noise source at the input of the VCO.

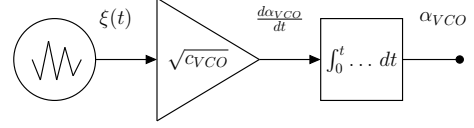


Fig. 2. Noise equivalent circuit diagram for a VCO, noise process  $\xi(t)$  from noise source input, scaled with  $\sqrt{c_{VCO}}$ , integral over differential time shifts yields process  $\alpha_{VCO}$

5. A shift in the control voltage of the oscillator at the input  $\Delta U$  corresponds linearly to a frequency shift  $\Delta f$ . The voltage sensitivity  $K_{VCO}$  in [Hz/V] is an oscillator-specific constant. The frequency of the oscillator output signal can then be expressed as

$$f = f_0 + \underbrace{K_{VCO}\Delta U(t)}_{\Delta f(t)}. \quad (11)$$

The output voltage signal can be described using the stochastic process  $\Delta f(t)$  representing the instantaneous frequency change as follows,

$$x_{VCO}(t) = \cos \left( 2\pi f_0 t + 2\pi \underbrace{\int_0^t \Delta f(\tau) d\tau}_{\phi(t)} + \phi_0 \right), \quad (12)$$

with  $\phi(t)$  referring to the phase shift process. The non-idealities of the noisy oscillator are characterized with regards to a stochastic time shift  $\alpha(t)$ . This time shift is connected to the phase shift and frequency shift such that

$$\alpha(t) = \frac{1}{2\pi f_0} \phi(t) = \frac{1}{f_0} \int_0^t \Delta f(t') dt'. \quad (13)$$

#### B. Free Running Oscillator - Discrete Time Domain Model

The model described here represents a free running oscillator in discrete time. As established previously, the stochastic time shift process of the oscillator can be modeled as a Wiener process. This process is a Gaussian process  $\xi$  of unit variance, scaled with the oscillator constant  $c_{VCO}$ . In discrete time, the process can be written as

$$\alpha_{VCO}[n] = \begin{cases} \xi(0) = 0, & n = 0 \\ \sqrt{c_{VCO}\Delta t} \sum_{i=0}^{n-1} \xi(i\Delta t), & n > 0 \end{cases}. \quad (14)$$

Defining  $\xi(0) = 0$  is a convention and has no significance on the statistical properties of the time shift process. The term  $\xi(i\Delta t)$  refers to increments at discrete time points  $i\Delta t$ , with  $\Delta t$  representing the sample interval. The corresponding phase shift process is then given as  $\phi_{VCO}[n] = 2\pi f_0 \alpha_{VCO}[n]$ .

#### C. Autocorrelation Function of Voltage Controlled Oscillator Output Process

In this subsection, the aim is to find an analytic expression for the ACF at the output of the noisy oscillator. This ACF can then be used to compute the PSD in the next step. The noise equivalent circuit diagram for a VCO is given in Fig. 2. An

ideal oscillator signal (cf. (1)) is a periodic signal that can be expressed by the Fourier series

$$x_0(t) = \sum_{i=-\infty}^{\infty} \underline{X}_i e^{ji2\pi f_0 t}, \quad (15)$$

with complex conjugate symmetric Fourier coefficients  $\underline{X}_i$ . The ACF of the noisy oscillator output for the first harmonic  $i = \pm 1$  is then given as

$$\begin{aligned} R_{x,x}(t, t + \tau) &= \mathbb{E}[x_0(t + \alpha(t))x_0^*(t + \tau + \alpha(t + \tau))] \\ &= \sum_{i=\pm 1} |\underline{X}_i|^2 e^{ji2\pi f_0 \tau} \mathbb{E}\left[e^{ji2\pi f_0 [\alpha(t) - \alpha(t + \tau)]}\right] \\ &\quad + \underline{X}_i \underline{X}_{-i}^* e^{ji2\pi f_0 (2t + \tau)} \mathbb{E}\left[e^{ji2\pi f_0 [\alpha(t) + \alpha(t + \tau)]}\right]. \end{aligned} \quad (16)$$

In the expression in (16), there is a term for a difference process  $\Delta\alpha = \alpha(t) - \alpha(t + \tau)$  and a sum process  $\Sigma\alpha = \alpha(t) + \alpha(t + \tau)$ . The corresponding characteristic functions<sup>1</sup> are specified to replace the terms of the expectation [12]

$$\Psi_{\Delta\alpha}(i2\pi f_0) = e^{-\frac{1}{2}(2\pi f_0)^2 \text{Var}(\Delta\alpha)}, \quad (17)$$

$$\Psi_{\Sigma\alpha}(i2\pi f_0) = e^{-\frac{1}{2}(2\pi f_0)^2 \text{Var}(\Sigma\alpha)}. \quad (18)$$

Using properties of the wiener process, the variance is found (c.f. [4, (32)]) with  $i = k, i \neq k$  respectively, assuming  $\tau > 0$ )

$$\text{Var}(\Delta\alpha) = \text{Var}(\alpha(t) - \alpha(t + \tau)) = c_{\text{VCO}}|\tau| \quad (19)$$

and for the sum process

$$\text{Var}(\Sigma\alpha) = \text{Var}(\alpha(t) + \alpha(t + \tau)) = c_{\text{VCO}}[4t + \tau]. \quad (20)$$

Note that the characteristic function for the sum process  $\Psi_{\Sigma\alpha}$  becomes asymptotically  $\lim_{t \rightarrow \infty} e^{-t} = 0$ . However, the characteristic function for the difference term  $\Psi_{\Delta\alpha}$  is independent of time. Then, the ACF asymptotic time invariant behaviour for  $t \rightarrow \infty$  can be obtained by inserting into (16).

$$\begin{aligned} \lim_{t \rightarrow \infty} R_{x,x}(t, t + \tau) &= \sum_{i=\pm 1} |\underline{X}_i|^2 e^{ji2\pi f_0 \tau} e^{-\frac{1}{2}(2\pi f_0)^2 c_{\text{VCO}}|\tau|} \\ &= R_{x,x}(\tau). \end{aligned} \quad (21)$$

#### D. Power Spectrum Density of Voltage Controlled Oscillator

The PSD of the disturbed oscillator output is computed by the Fourier transform  $S_{x,x}(f) = \mathfrak{F}_\tau\{R_{x,x}(\tau)\}$ , and given by

$$S_{x,x}(f) = \sum_{i=\pm 1} |\underline{X}_i|^2 \frac{f_0^2 c_{\text{VCO}}}{(f + if_0)^2 + \pi^2 f_0^4 c_{\text{VCO}}^2}. \quad (22)$$

The PSD shape of the oscillator output is a Lorentzian, shifted by the oscillator frequency  $f_0$  (cf. noisy oscillator output spectrum around first harmonic, Fig. 3). The phase noise of the oscillator has the effect of spreading the spectrum of the dirac pulse which represents the PSD of ideal oscillator. The spectral spreading is characterized by  $c_{\text{VCO}}$  of the oscillator. To obtain the single-sideband phase noise spectrum  $\mathcal{L}(f_{\text{offs}})$ ,

<sup>1</sup>characteristic function  $\Psi_Z(t) = \mathbb{E}[e^{jtZ}]$  of Gaussian-distributed random variable  $Z$

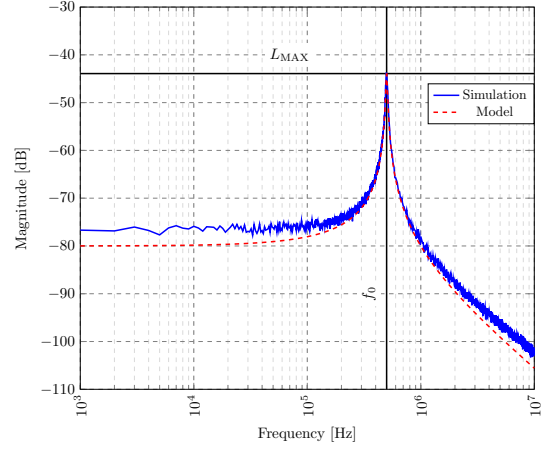


Fig. 3. Noisy oscillator output magnitude spectrum  $|S_{x,x}(f)|^2$  around first harmonic,  $f_0 = f_{\text{VCO}} = 500$  kHz,  $f_s = 100$  MHz sampling frequency,  $N = 100$  k samples,  $c_{\text{VCO}} = 10^{-11}$  s oscillator constant

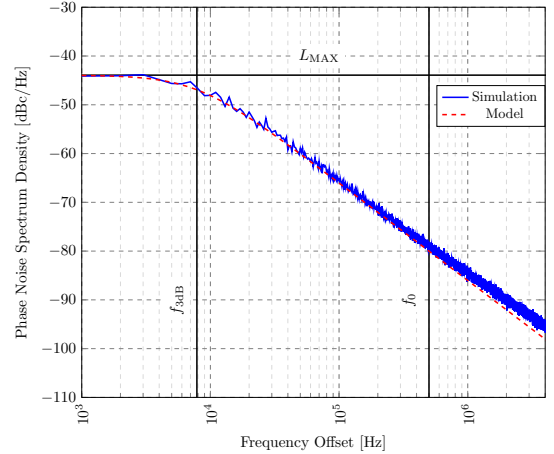


Fig. 4. Phase noise spectrum,  $f_0 = f_{\text{VCO}} = 500$  kHz,  $f_s = 100$  MHz sampling frequency,  $N = 100$  k samples,  $c_{\text{VCO}} = 10^{-11}$  s oscillator constant

(22) is normed to the power at the first harmonic with  $f_{\text{offs}}$  frequency offset to carrier (see Fig. 4)

$$\begin{aligned} \mathcal{L}(f_{\text{offs}}) &= 10 \log_{10} \left( \frac{S_{x,x}(f_0 + f_{\text{offs}})}{\sum_{i=\pm 1} |\underline{X}_i|^2} \right) \\ &= 10 \log_{10} \left( \frac{f_0^2 c_{\text{VCO}}}{f_{\text{offs}}^2 + \pi^2 f_0^4 c_{\text{VCO}}^2} 1 \text{ Hz} \right) \text{ dBc/Hz}. \end{aligned} \quad (23)$$

The maximum PSD component can be found where the offset frequency becomes zero,

$$\mathcal{L}_{\text{MAX}} = -10 \log_{10} (\pi^2 f_0^2 c_{\text{VCO}}). \quad (24)$$

In Fig. 4, the low-pass characteristic of the phase noise PSD can be observed. The term  $f_{3\text{dB}} = \pi f_0^2 c_{\text{VCO}}$  refers to the 3 dB cut-off frequency. In the literature, this cut-off frequency is also known as *phase noise bandwidth* [13].

#### IV. PHASE-LOCKED LOOP

In this section the description of a free running oscillator is extended to a PLL circuit. In this part, a system model for the phase noise of a PLL is established. A PLL is typically

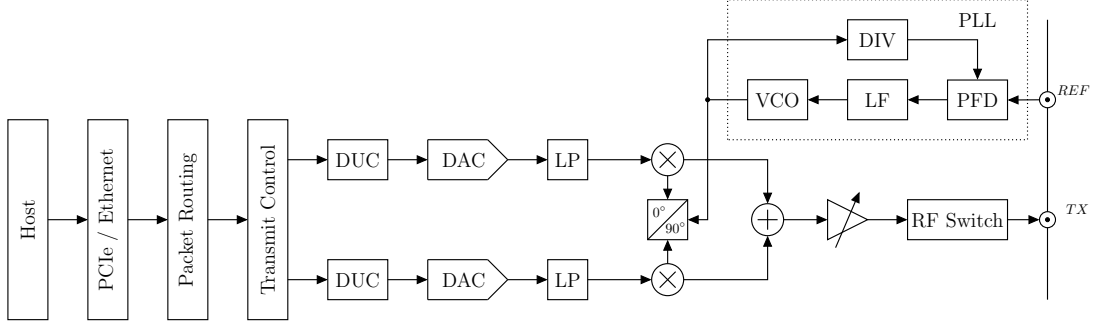


Fig. 5. Block diagram of the TX RF Chain for a generic USRP, PLL receives input from REF port, the PLL consists of PFD, LF, VCO and a frequency divider

used in the RF chain of a SDR device to synthesize the desired carrier frequency (cf. Fig. 5). The PLL circuit is a control loop that combines the dynamic adjustability of a VCO's output frequency with the favorable phase noise characteristics of a reference oscillator.

#### A. Phase-Locked Loop Model - Components and Basics

Fig. 6 shows the PLL circuit with all its components. In the figure,  $x_{\text{REF}}$ ,  $\Delta x$ ,  $\Delta \bar{x}$ ,  $x_{\text{PLL}}$ ,  $\tilde{x}_{\text{PLL}}$  represent time dependent voltage signals. The terms  $\alpha_{\text{REF}}$ ,  $\beta$ ,  $\gamma$ ,  $\alpha_{\text{VCO}}$ ,  $\alpha_{\text{PLL}}$  refer to stochastic time shift processes affecting the voltage signals. The output signal of the PLL is given as

$$\begin{aligned} x_{\text{PLL}}(t) &= \cos[2\pi f_{\text{PLL}}(t + \alpha_{\text{PLL}}(t))] \\ &= \cos[2\pi f_{\text{PLL}}t + \theta_{\text{PLL}}(t)]. \end{aligned} \quad (25)$$

The signal after the frequency divider is

$$\begin{aligned} \tilde{x}_{\text{PLL}}(t) &= \cos\left[2\pi \underbrace{\frac{f_{\text{PLL}}}{M}}_{=f_{\text{REF}}}(t + \alpha_{\text{PLL}}(t))\right] \\ &= \cos[2\pi f_{\text{PLL}}t + \tilde{\theta}_{\text{PLL}}(t)]. \end{aligned} \quad (26)$$

The PFD compares the phases of its input signals

$$\begin{aligned} \Delta\theta(t) &= \tilde{\theta}_{\text{PLL}}(t) - \theta_{\text{REF}}(t) \\ &= 2\pi f_{\text{REF}} \underbrace{(\alpha_{\text{PLL}}(t) - \alpha_{\text{REF}}(t))}_{=\beta(t)}. \end{aligned} \quad (27)$$

Its output signal  $\Delta x(t)$  is a pulse-width modulated signal whose duty cycle depends on  $\Delta\theta(t) \sim \beta(t)$  and is scaled

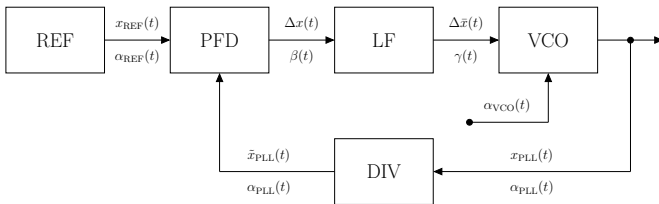


Fig. 6. PLL circuit diagram, REF reference signal oscillator, PFD phase frequency detector, LF loop filter, VCO voltage controlled oscillator, DIV frequency divider

with the phase detector gain  $k_{\text{PFD}}$

$$\Delta x(t) = k_{\text{PFD}} \sum_{k=0}^{\infty} \text{rect}\left(\frac{t - 0.5\beta(\frac{k}{f_{\text{REF}}})}{\beta(\frac{k}{f_{\text{REF}}})}\right) * \delta(t - \frac{k}{f_{\text{REF}}}). \quad (28)$$

The idea of a LF is to balance the effect of the previous differentiation step in the PFD to improve the stability of the control loop. Therefore, a LF is typically a filter that can be a low-pass filter (LPF) of first order, second order or a charge pump that sums up the error signal  $\Delta x(t)$ . Its output is a low-pass (LP)-filtered error signal  $\Delta \bar{x}(t) = h_{\text{LF}}(t) * \Delta x(t)$  with corresponding time shift process  $\gamma(t)$ . The VCO input is the filtered error signal  $\Delta \bar{x}(t + \gamma(t))$  as the control voltage, affected by a corresponding filtered stochastic time shift. Furthermore, the VCO has its own phase noise process, represented by the stochastic time shift  $\alpha_{\text{VCO}}(t)$ .

The assumptions for the considered PLL model are [5]:

1. The PLL is locked, i.e.  $f_{\text{REF}} \approx f_{\text{PLL}}/M$ , with frequency of reference signal  $f_{\text{REF}}$ , PLL output frequency  $f_{\text{PLL}}$  and divider ratio  $M$ .
2. The input of the PLL is a reference signal source which is modeled as a free running oscillator)

$$\begin{aligned} x_{\text{REF}}(t) &= \cos[2\pi f_{\text{REF}}(t + \alpha_{\text{REF}}(t))] \\ &= \cos[2\pi f_{\text{REF}}t + \theta_{\text{REF}}(t)]. \end{aligned} \quad (29)$$

3. All the noise sources in the PLL circuit are zero mean white Gaussian and are independent of each other.

#### B. Phase Noise in Phase-Locked Loops

Fig. 7 shows the noise equivalent block diagram for the PLL. It is assumed that other components (divider, loop filter, etc.) besides the oscillators are noise free. In the simple case, where no loop filter is present and we consider two noise sources ( $p = 1, q = 2$ ), the system of differential equations can be written as (c.f. (51))

$$\begin{aligned} \frac{d}{dt} \underbrace{\beta(t)}_{\mathbf{y}} &= - \underbrace{\sqrt{c_{\text{CTL}}} k_{\text{PFD}}}_{\mathbf{A}} \underbrace{\beta(t)}_{\mathbf{y}} \\ &+ \underbrace{[\sqrt{c_{\text{VCO}}} \quad -\sqrt{c_{\text{REF}}}]_{\mathbf{B}}}_{\mathbf{B}} \underbrace{\begin{bmatrix} \xi_{\text{VCO}}(t) \\ \xi_{\text{REF}}(t) \end{bmatrix}_{\mathbf{\xi}}}_{\mathbf{\xi}}. \end{aligned} \quad (30)$$

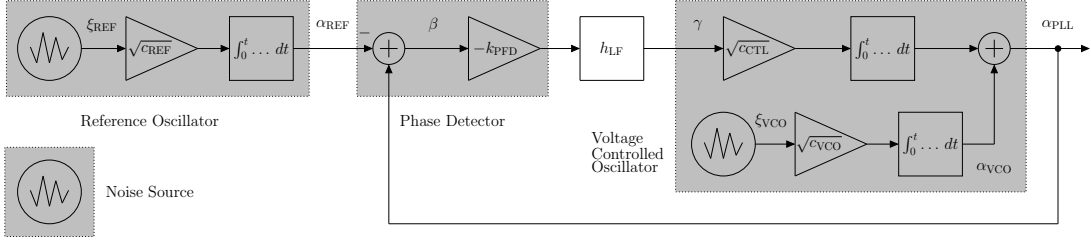


Fig. 7. Noise equivalent block diagram for PLL [14], considering white noise sources effecting the control voltage of reference oscillator and VCO

The characterization of a generic PLL and derivation of the system of differential equations representing the PLL dynamics is shown in Appendix A. In the considered case of a first order PLL, with  $\sqrt{c_{CTL}}k_{PFD} = \omega_{PLL} = 2\pi f_{PLL}$ , the solution to (30) is

$$\beta(t) = \int_0^t e^{-2\pi f_{PLL}(t-t')} (\sqrt{c_{VCO}}\xi_{VCO}(t) - \sqrt{c_{REF}}\xi_{REF}(t)) dt. \quad (31)$$

### C. Discrete Time Domain Model

The model described here represents a PLL in the discrete time. The time index is represented by variables  $i, n$  and the sample interval is denoted by  $\Delta t$ . In discrete time, the time shift process at the PLL output can be expressed as (cf. (30) by substituting  $\alpha[i] = \sqrt{c} \int_0^i \xi(t) dt$ ), such that

$$\alpha_{PLL}[n] = \begin{cases} 0, & n = 0 \\ \sum_{i=0}^{n-1} (\alpha_{PLL}[i] - \alpha_{REF}[i]) \cdot (-2\pi f_{PLL} \Delta t) + \alpha_{VCO}[n-1], & n > 0 \end{cases}. \quad (32)$$

Note that this process becomes stationary when  $\alpha_{REF}$  becomes constant. Identical to the case of a free running oscillator, the corresponding phase shift process at PLL output becomes  $\phi_{PLL}[n] = 2\pi f_0 \alpha_{PLL}[n]$ .

### D. Autocorrelation Function of Phase-Locked Loop Output Process

Similar to the approach for describing a free running VCO previously, the following step is to obtain the ACF for the process at the PLL output. With (54) and (10) the ACF can be written as

$$\begin{aligned} R_{\alpha,\alpha}(t, t+\tau) &= \mathbb{E}[\alpha_{PLL}(t)\alpha_{PLL}(t+\tau)] \\ &= c_{REF} \min(t, t+\tau) + R_{\alpha,\beta}(t, t+\tau) \\ &\quad + R_{\beta,\alpha}(t, t+\tau) + R_{\beta,\beta}(t, t+\tau). \end{aligned} \quad (33)$$

Further derivation steps are given in the Appendix B. The ACF of  $\alpha_{PLL}$  at the PLL output is

$$\begin{aligned} R_{\alpha,\alpha}(t, t+\tau) &= \frac{c_{VCO} + c_{REF}}{4\pi f_{PLL}} \left[ e^{-2\pi f_{PLL}|\tau|} - e^{-2\pi f_{PLL}(2t+\tau)} \right] \\ &\quad - \frac{c_{REF}}{2\pi f_{PLL}} \left[ e^{-2\pi f_{PLL}|\tau|} - e^{-2\pi f_{PLL}(t+\tau)} + 1 - e^{-2\pi f_{PLL}t} \right] \\ &\quad + c_{REF}t. \end{aligned} \quad (34)$$

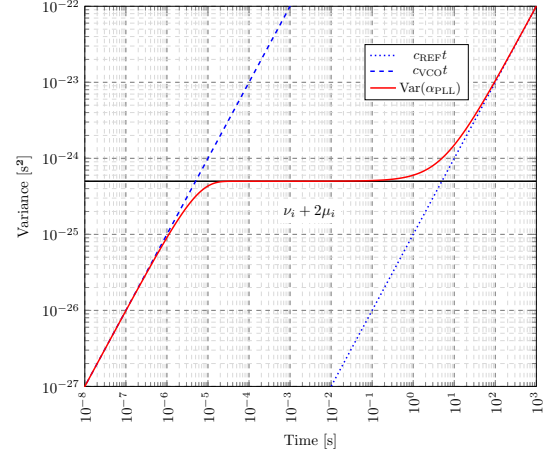


Fig. 8. Variances for PLL and free running oscillators REF and VCO for  $c_{REF} = 10^{-16}$  s,  $c_{VCO} = 10^{-14}$  s,  $2\pi f_{PLL} = 10^5$  rad  $\cdot$  s $^{-1}$

### E. Variance of Phase-Locked Loop Output Process

In order to illustrate the key characteristic of the ACF, in this subsection the Variance of the PLL time shift output process is plotted in Fig. 8. The variance of the output process  $\alpha_{PLL}$  is found for  $\tau = 0$  of its ACF (34)

$$\text{Var}(\alpha_{PLL}(t)) = R_{\alpha,\alpha}(t, \tau = 0). \quad (35)$$

In the case of a first order PLL (no LF) the expression becomes

$$\begin{aligned} \text{Var}(\alpha_{PLL}) &= \frac{c_{VCO} + c_{REF}}{4\pi f_{PLL}} [1 - e^{-4\pi f_{PLL}t}] \\ &\quad - 2 \frac{c_{REF}}{2\pi f_{PLL}} [1 - e^{-2\pi f_{PLL}t}] + c_{REF}t \\ &\approx \frac{c_{VCO} - 3c_{REF}}{4\pi f_{PLL}} [1 - e^{-4\pi f_{PLL}t}] + c_{REF}t. \end{aligned} \quad (36)$$

Fig. 8 illustrates the behaviour of the variance given by (36). For smaller times, the PLL variance follows that of a free running oscillator VCO. Between  $10^{-5}$  s to  $10^{-1}$  s the variance remains constant at  $\nu_i + 2\mu_i = \frac{c_{VCO} - 3c_{REF}}{4\pi f_{PLL}}$ . Note that this behaviour is explained by Ornstein-Uhlenbeck (OU) process  $\beta(t)$  having a constant variance. At larger times ( $> 10^2$  s) the contribution from the  $c_{REF}t$  term in (36) becomes significant and the variance of the PLL follows that of the REF oscillator.

### F. Power Spectrum Density of Phase-Locked Loop

For deriving the phase noise spectrum of the PLL, a similar approach to previous derivation for the VCO will be taken. The



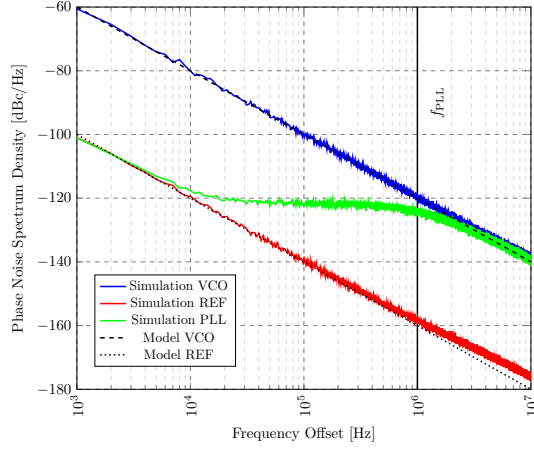


Fig. 9. Phase noise of PLL, free running VCO and REF, parameters  $c_{\text{REF}} = 10^{-16}$  s,  $c_{\text{VCO}} = 10^{-14}$  s,  $f_{\text{PLL}} = k_{\text{PFD}}\sqrt{c_{\text{CTL}}}/2\pi = 10^6$  Hz,  $f_s = 10^8$  Hz and  $N = 100$  k samples

full derivation is provided in Appendix C. Similar to (15), a Fourier series expression for the ideal oscillator signal is used. The ACF of the PLL output signal  $x_{\text{PLL}}(t) = x_0(t + \alpha_{\text{PLL}}(t))$  around the first harmonic is

$$R_{x,x}(t, t + \tau) = \mathbb{E}[x_0(t + \alpha_{\text{PLL}}(t))x_0^*(t + \tau + \alpha_{\text{PLL}}(t + \tau))]. \quad (37)$$

Then, the asymptotic ACF of the  $\alpha_{\text{PLL}}$  process can be written as

$$\lim_{t \rightarrow \infty} R_{x,x}(t, t + \tau) = \sum_{i=\pm 1} |X_i|^2 e^{j2\pi f_0 \tau} \cdot e^{-(2\pi f_0)^2 \left[ \frac{c_{\text{VCO}} - c_{\text{REF}}}{4\pi f_{\text{PLL}}} [1 - e^{-2\pi f_{\text{PLL}}|\tau|}] + 0.5c_{\text{REF}}|\tau| \right]}. \quad (38)$$

The PSD of the PLL output is

$$\begin{aligned} S_{x,x}(f) &= \mathfrak{F}_\tau \left\{ R_{x,x}(\tau) \right\} \\ &= \sum_{i=\pm 1} |X_i|^2 \sum_{n=0}^{\infty} \frac{1}{n!} e^{-\frac{\pi f_0^2}{f_{\text{PLL}}} (c_{\text{VCO}} - c_{\text{REF}})} \\ &\quad \cdot \left( \frac{\pi f_0^2}{f_{\text{PLL}}} (c_{\text{VCO}} - c_{\text{REF}}) \right)^n \\ &\quad \cdot \frac{4\pi (\pi f_0^2 c_{\text{REF}} + n f_{\text{PLL}})}{(2\pi (\pi f_0^2 c_{\text{REF}} + n f_{\text{PLL}}))^2 + (f - i f_0)^2}. \end{aligned} \quad (39)$$

Comparing the phase noise spectrum for the output of a noisy PLL to that of a free running oscillator (22):

- The expression of the spectrum consists a Dirac-pulse  $\delta(f)$  for the ideal oscillator spread by phase noise.
- The spectrum consists of a (weighted) sum of Lorentzian spectrum's, shifted by frequency  $f_0$  of the VCO in the PLL

In Fig. 9, the phase noise spectrum of the PLL circuit is shown. Note that for low frequencies, the PLL follows the behavior of the free running REF oscillator. The PLL bandwidth  $f_{\text{PLL}}$  characterizes the frequency after which it follows the behavior of a free running VCO asymptotically. During the transition interval up to the PLL bandwidth, the spectrum is nearly constant. For the model of VCO and REF the general derivation

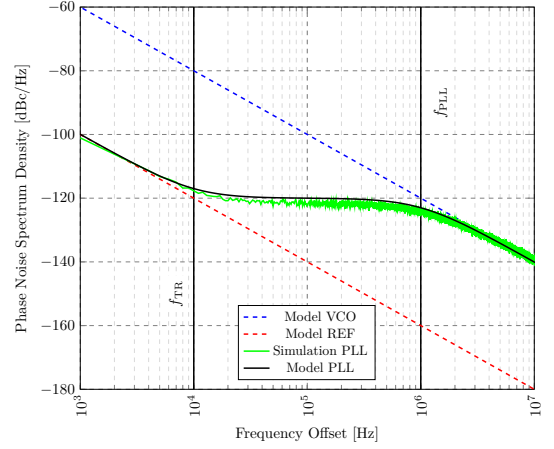


Fig. 10. Phase noise of PLL, comparing simplified phase noise model with simulation, identical parameters to Fig. 9,  $f_{\text{TR}} = 10^4$  Hz

for a free running VCO in (23) is used.

### G. Simplified Expression for Phase Noise Spectrum of Phase-Locked Loops

The next step is simplifying the expression (39) for the PLL output PSD. The sum of Lorentzian spectrums shall be reduced to the minimum number of necessary components. From Fig. 10, it can be seen that for low offset frequencies, the PLL follows the characteristic of the REF oscillator. The REF oscillators phase noise is described by (cf. (23), units omitted)

$$\begin{aligned} \mathcal{L}_{\text{REF}}(f_{\text{offs}}) &= 10 \log_{10} \left( \frac{f_0^2 c_{\text{REF}}}{f_{\text{offs}}^2 + \pi^2 f_0^4 c_{\text{REF}}^2} \right) \\ &= 10 \log_{10} \left( \frac{1}{\pi^2 f_0^2 c_{\text{REF}}} \frac{1}{1 + \frac{f_{\text{offs}}^2}{f_{\text{3dB,REF}}^2}} \right). \end{aligned} \quad (40)$$

During the transition interval, starting at frequency  $f_{\text{TR}}$  the spectrum remains constant until the PLL bandwidth  $f_{\text{PLL}}$ . For higher frequencies, PLL follows the characteristic of the VCO, given by (cf. (23))

$$\mathcal{L}_{\text{VCO}}(f_{\text{offs}}) = 10 \log_{10} \left( \frac{1}{\pi^2 f_0^2 c_{\text{VCO}}} \frac{1}{1 + \frac{f_{\text{offs}}^2}{f_{\text{3dB,VCO}}^2}} \right). \quad (41)$$

The unknown frequency  $f_{\text{TR}}$  can be obtained by first calculating  $\mathcal{L}_{\text{VCO}}(f_{\text{offs}} = f_{\text{PLL}})$ . Then, the equation  $\mathcal{L}_{\text{VCO}}(f_{\text{offs}} = f_{\text{PLL}}) = \mathcal{L}_{\text{REF}}(f_{\text{offs}} = f_{\text{TR}})$  can be solved for  $f_{\text{TR}}$ . For the choice of parameters given in caption Fig. 9 we obtain  $f_{\text{TR}} = 10^4$  Hz. To have a more general expression the exponents in each component are expressed as a variable  $k_{\text{VCO}}, k_{\text{REF}}$  for the slope of the LP filters representing the VCO and REF. In our derivation, assuming white noise sources, the variables are  $k_{\text{VCO}} = k_{\text{REF}} = 2$ , which leads to a slope of  $-20 \frac{\text{dBc}}{\text{Hz} \cdot \text{decade}}$ . However, this might not reflect the characteristic of a specific VCO or REF appropriately, which necessitates a generic expression. Finally the simplified expression for the phase

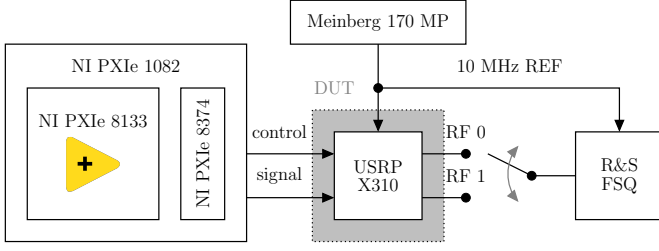


Fig. 11. Setup for measuring the phase noise spectrum of SDR USRP X310 with reference clock Meinberg 170 MP

noise spectrum can be expressed as

$$\mathcal{L}_{\text{PLL}}(f_{\text{offs}}) = 10 \log_{10} \left[ \frac{1}{\pi f_{3\text{dB,REF}}} \cdot \frac{1 + \left( \frac{f_{\text{offs}}}{f_{\text{TR}}} \right)^{k_{\text{REF}}}}{1 + \left( \frac{f_{\text{offs}}}{f_{3\text{dB,REF}}} \right)^{k_{\text{REF}}}} \cdot \frac{1}{1 + \left( \frac{f_{\text{offs}}}{f_{\text{PLL}}} \right)^{k_{\text{VCO}}} } \right]. \quad (42)$$

This PLL model is illustrated in Fig. 10 by the black plot.

## V. MEASUREMENT

The aim in the following parts is to provide a framework for fitting the previously outlined system model to specific hardware. This is done to create a meaningful connection between theory and practical reality. To achieve this, measurements of the phase noise spectrum of common SDR devices are recorded. The SDR investigated in this work are variants of the commonly in mobile communication research and development used NI USRP X310.

### A. Measurement Setup

Fig. 11 shows the phase noise measurement setup. The LabVIEW program running on the NI PXIe 8133 controller generates the digital signal and provides control over signal parameters. This signal is streamed to the SDR device over the NI PXIe 8374 interface. The streaming interface and controller are mounted in a NI PXIe 1082 chassis. The LabVIEW controller provides control over signal parameters such as bandwidth, carrier frequency and power/gain. For the measurements, a constant value baseband signal is generated to allow observation of the signal synthesized by the PLL. Both the USRP and the spectrum analyzer R&S FSQ used to perform the phase noise spectrum measurement are connected to the same 10 MHz REF from a Meinberg 170 MP GPS receiver. The common reference oscillator is essential to ensure frequency synchronicity between DUT and R&S FSQ. The USRP RF port, for which the signal is generated, is directly connected to the R&S FSQ via coaxial cable.

### B. Measurement Setup Configuration

The key parameters of the USRP configuration are outlined in Table I. The carrier frequencies are selected from a broad range to capture the performance characteristics across different operating conditions. Since the digital baseband signal is

Property	Value
Carrier freq. (MHz)	{500, 2000, 5000}
Bandwidth (MHz)	10
Power (dBm)	0
Waveform	constant value
Port	{RF0, RF1} TX
Reference (MHz)	10

TABLE I  
USRP CONFIGURATION

set as a constant value to obtain the oscillator signal at the RF ports, the bandwidth plays a minor role and is set arbitrarily to 10 MHz. The phase noise spectrum measurement is performed for both RF chains, due to each USRP being equipped with two RF frontend daughterboards.

### C. Phase Noise Spectrum Measurements

In this subsection, the phase noise measurements for various USRP models in different configurations is detailed. The measured dataset [15] of phase noise spectrums contains data for the following USRP models:

- USRP 2944R (160 MHz, UBX daughterboard)
- USRP 2953R (120 MHz, CBX daughterboard)
- USRP 2953R (40 MHz, CBX daughterboard)
- USRP 2954R (160 MHz, UBX daughterboard)

In separate measurements, a 30 dB attenuator is placed in front of the FSQ's input, to explore the effect on measured phase noise.

In Fig. 12, USRPs with UBX and CBX daughterboards are compared. It can be seen that while the PLL bandwidth  $f_{\text{PLL}}$  and  $f_{\text{TR}}$  are slightly different, however, the overall characteristic of the phase noise spectrum remains similar. This is expected given that the phase noise characteristics of their frequency synthesizing circuits (Maxim Integrated MAX2870 for CBX and MAX2871 for UBX) are identical [16], [17]. The observed difference in the phase noise spectrum likely originate from different wiring and circuitry connecting the PLL and other RF components on the daughter- and motherboards, more specifically the LF.

In Fig. 13 the effect of different carrier frequencies on phase noise PSD is explored. The observable increase of the PSD results from the phase noise scaling multiplicatively with oscillator frequency (42). In the green plot, a 30 dB attenuator is introduced to assess its impact on phase noise measurements. It can be seen that this effectively raises the noise floor from  $-135 \text{ dBc/Hz}$  to  $-115 \text{ dBc/Hz}$  in the measurement. This results from the attenuator reducing the signal power fed to the FSQ. Since the FSQ has an inherent fixed noise floor level given by its hardware properties, the effect is a raised observed noise floor in the measurement. However, the overall phase noise characteristic of the USRP output signal is not affected by the attenuator. This is due to the PSD representing the power density relative to the carrier power. The relation is maintained as long as the absolute signal power does not fall below the detection limit of the FSQ, at which point the PSD gradually submerges in the noise floor.



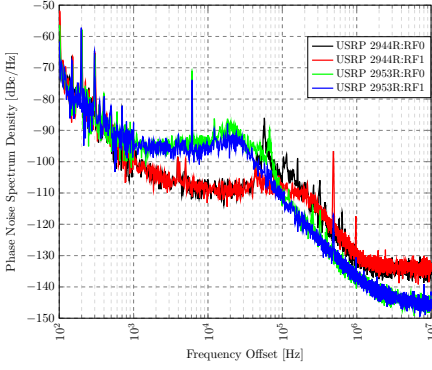


Fig. 12. Measured phase noise spectrum [15] for USRP with different daughterboards - 2944R (UBX) and 2953R (CBX) at  $f_c = 2$  GHz

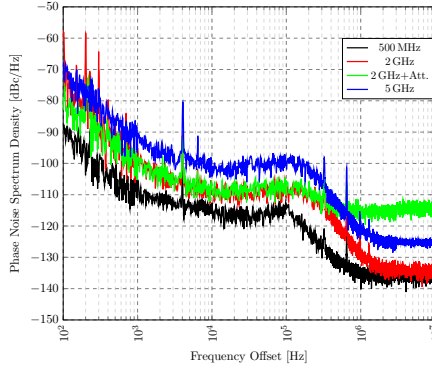


Fig. 13. Measured phase noise spectrum [15] for USRP 2944R (UBX) at different frequencies

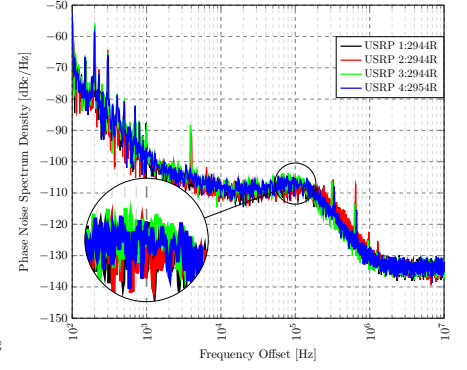


Fig. 14. Measured phase noise spectrum [15] of different USRP with identical daughterboards at  $f_c = 2$  GHz

In Fig. 14 the phase noise spectrum of different USRP with identical daughterboards UBX is shown. It can be observed that the characteristics of the PSD's are practically identical, suggesting that phase noise behaviour is consistent among different USRP with the same daughterboard type. This insight is important when phase coherent operation of multiple USRP's is desired. Sufficiently similar phase noise characteristics are important to simplify phase synchronization efforts. This is due to typical synchronization methods, such as suppression of phase noise with Kalman filtering relying on estimating the statistical moments of the phase noise processes [13]. When the spectral characteristics are distinct, these statistical moments can be significantly different, hindering phase synchronization efforts.

#### D. Discussion

This subsection is dedicated to discussing the differences and their causes between the model (42), highlighted in Fig. 10 and the measured PSD's in Fig. 12, 13, 14. While the overall spectrum shape in measurements is similar, specific differences can be noted. Most notable is a difference in the slope of the spectrum ( $-30 \frac{\text{dBc}}{\text{Hz} \cdot \text{decade}}$  in measurements and  $-20 \frac{\text{dBc}}{\text{Hz} \cdot \text{decade}}$  in the model). The slope observed in the measurements is identical to the datasheets [16, p. 5] [17, p. 6] in "VCO open loop phase noise" for the PLL circuits, which supports the credibility of the measurement. This difference results from other influences, besides white noise sources affecting the control voltage, affecting the phase noise characteristic of VCO and REF oscillators. However, using the generic simplified model (42) allows to fit the parameters  $k_{\text{VCO}}, k_{\text{REF}}$  to match the specific characteristics of the oscillators. The transition interval between REF and VCO dominant parts in the measured PSD is not completely flat as in the model. This difference occurs since the derivation assumed absence of a LP filter for simplicity. The datasheet figures [16, p. 5] [17, p. 6] in "closed loop phase noise" exhibit identical characteristics to our measurements. Another difference is that the measurement contains spurs, while the model does not account for this effect. The spurs visible in a PLL's PSD originate from various sources such as non-linearities in circuits, unwanted mixing products and over-driving RF

components [18]. Furthermore, the measured PSD shows less smoothness in its low-frequency components compared to the model, primarily due to the limited measurement time-frame. The total sweep time of 25 s is evidently not sufficient so that low frequency components are adequately represented in the measured spectrum. A practical solution to address this limitation is to record multiple measurements and average the measured PSDs in post-processing.

## VI. PARAMETER ESTIMATION

In this section, the measured PSDs are used to estimate the parameters of the simplified model (42). The primary interest is in the oscillator constant for VCO and REF,  $c_{\text{VCO}}, c_{\text{REF}}$  and the corresponding 3 dB cut-off frequencies, frequency at the start of the transition interval  $f_{\text{TR}}$  and PLL bandwidth  $f_{\text{PLL}}$ . The established system model is extended to account for the noise floor that was not considered in the derivation. Estimators for the system model parameters are presented and explicitly calculated for the recorded data-set. Note that the notations used in the system model (42) are shortened here to  $\mathcal{L}_{\text{PLL}} = \mathcal{L}$  and  $f_{\text{offs}} = f$ . Furthermore, the accent  $\hat{f}_{\text{TR}}$  is used to indicate parameter estimates.

### A. System Model Extension

Since the frequency response of all oscillators contains a noise floor, a noise floor is added to the system model with  $\mathcal{L}_{\text{max}} = -10 \log_{10}(\pi f_{3\text{dB,REF}})$  (c.f. 24)

$$\mathcal{L}(f) = \mathcal{L}_{\text{max}} + 10 \log_{10} \left[ \frac{1 + \left(\frac{f}{f_{\text{TR}}}\right)^{k_{\text{REF}}}}{1 + \left(\frac{f^2}{f_{3\text{dB,REF}}^2}\right)^{k_{\text{REF}}}} \cdot \frac{1 + \left(\frac{f}{f_{\text{NF}}}\right)^{k_{\text{VCO}}}}{1 + \left(\frac{f^2}{f_{\text{PLL}}^2}\right)^{k_{\text{VCO}}}} \right]. \quad (43)$$

The noise floor of any oscillator can be observed at sufficiently large frequency offsets  $f_{\text{NF}}$  relative to the oscillator frequency. Note that the measured noise floor depends on the oscillator but also the sensitivity of the device used to measure the phase noise. The datasheet for the oscillator used on the UBX daughterboard [17, p. 6] and conducted measurements suggest that the slope of the phase noise spectrum is  $-30 \frac{\text{dBc}}{\text{Hz} \cdot \text{decade}}$ .

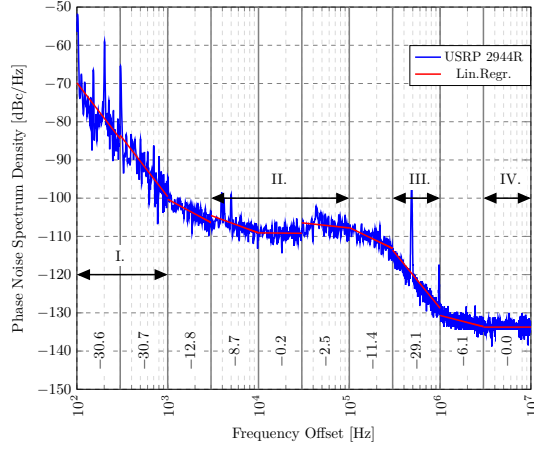


Fig. 15. Phase noise spectrum of USRP 2944R with UBX daughterboard in blue, piece-wise linear regression in red and corresponding estimates of slope  $\hat{R}[1]$  in  $\left[\frac{\text{dBc}}{\text{Hz-decade}}\right]$  given at the bottom of the plot

Therefore, the exponents in the system model are adjusted appropriately  $k_{\text{REF}} = k_{\text{VCO}} = 3$ . While in (43) the 3dB frequency of the VCO  $f_{3\text{dB,VCO}}$  is not explicitly included, it is implicitly contained in  $f_{\text{TR}}$  which was introduced in (42) to allow for more concise notation

$$f_{\text{TR}} = f_{3\text{dB,REF}} \sqrt{\frac{f_{3\text{dB,VCO}}^2 + f_{\text{PLL}}^2}{f_{3\text{dB,VCO}} \cdot f_{3\text{dB,REF}}} - 1} \quad (44)$$

in the case of  $k_{\text{VCO}} = k_{\text{REF}} = 2$  and in the general case

$$f_{\text{TR}} = \sqrt[k_{\text{REF}}]{\frac{f_{3\text{dB,VCO}}^{k_{\text{VCO}}} + f_{\text{PLL}}^{k_{\text{VCO}}}}{f_{3\text{dB,VCO}}} f_{3\text{dB,REF}} - f_{3\text{dB,REF}}^{k_{\text{REF}}}} \quad (45)$$

Note that these expressions are derived from (43) by neglecting non significant components and solving for the desired intersection point frequency (cf. Fig. 16).

### B. Analyzing PSD Characteristics

Before the parameters of the system model can be estimated, the PSD has to be split up in the following characteristic parts: 1) REF dominant influence, 2) transition interval, 3) VCO dominant influence, and 4) noise floor. To achieve this, the slope of the PSD is estimated using linear regression. Fig. 15 shows a piece-wise linear regression of the phase noise spectrum given by

$$\hat{\mathbf{R}} = (\mathbf{X}^T \mathbf{X})^{-1} \mathbf{X}^T \mathbf{Y}. \quad (46)$$

The matrix

$$\mathbf{X} = \begin{bmatrix} 1 & \cdots & 1 \\ \log_{10}(f_0) & \cdots & \log_{10}(f_n) \end{bmatrix} \quad (47)$$

contains the logarithmized bounds of the segment for which the regression is calculated, while  $\mathbf{Y} = [\mathcal{L}(f_0), \dots, \mathcal{L}(f_n)]$  represents the corresponding magnitude values of the phase noise spectrum. Clearly distinguishable are the following sections:

1.  $f < 1 \text{ kHz}$ : PLL follows REF
2.  $3 \text{ kHz} \leq f \leq 100 \text{ kHz}$ : PLL in transition period

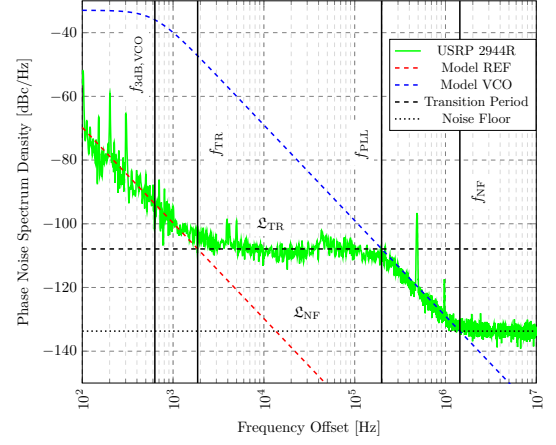


Fig. 16. Phase noise spectrum of USRP 2944R with parameter estimates and fitted models for REF and VCO

3.  $300 \text{ kHz} \leq f \leq 1 \text{ MHz}$ : PLL follows VCO
4.  $f > 3 \text{ MHz}$ : noise floor

### C. Estimators for Phase Noise Model Parameters

This subsection is dedicated to estimating the parameters mentioned in the start of the section. Explicit numerical values for parameter estimates are given in Appendix D. To estimate the oscillator constants, it is necessary to first estimate the cut-off frequencies for the LP representing the phase noise characteristic of VCO and REF. A general expression for the 3dB cut-off frequency estimate can be derived from (40),

$$\hat{f}_{3\text{dB}} = 10^{\frac{1}{k-1} \sum_{n=0}^N \log_{10}(10^{\mathcal{L}_n/10} \pi f_n^k)}. \quad (48)$$

Note that the relation  $f_{\text{offs}} = f \gg f_{3\text{dB}}$  is used for simplification in separating the variable. Furthermore,  $\mathcal{L}_n$  is equivalent to  $\mathcal{L}(f_n)$  and  $k \in \{k_{\text{REF}}, k_{\text{VCO}}\}$ . By summing over logarithmic values, the effect of spurs on the parameter estimate is reduced.

The estimator for the 3dB cut-off frequency (48) is used on the intervals where the REF and VCO are dominant. For the measurement displayed in Fig. 15, this yields the estimate for the 3dB cut-off frequency of REF  $\hat{f}_{3\text{dB,REF}}$  and VCO  $\hat{f}_{3\text{dB,VCO}}$ . As the oscillator frequency during the measurement is known, the oscillator constants can be derived by the following relation

$$\hat{c} = \frac{f_{3\text{dB}}}{\pi f_0^2}.$$

The next objective is to estimate the frequency where the transition interval starts  $f_{\text{TR}}$ , PLL bandwidth  $f_{\text{PLL}}$  and the frequency where the noise floor starts  $f_{\text{NF}}$ . To achieve this, first the power level of the transition interval and the noise floor is estimated. This power level estimate is obtained via the sample mean estimator

$$\hat{\mathcal{L}} = \frac{1}{N} \sum_{n=0}^N \mathcal{L}_n. \quad (49)$$

Using this estimator, the estimated power levels for transition interval  $\hat{\mathcal{L}}_{\text{TR}}$  and noise floor  $\hat{\mathcal{L}}_{\text{NF}}$  are obtained. The desired

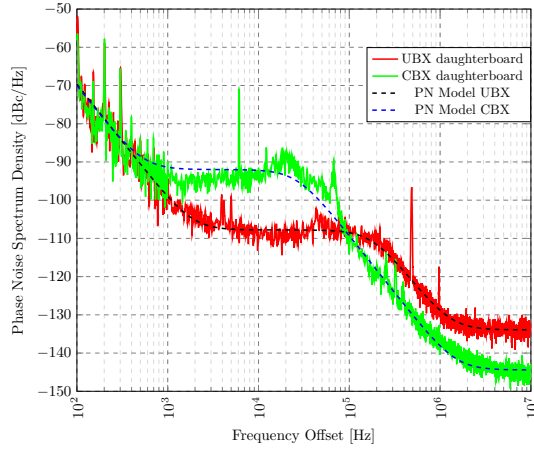


Fig. 17. Phase noise spectrum of the system model using the derived parameter estimates for each daughterboard

frequencies can then be found at the intersection point of the power levels  $\hat{\mathcal{L}}$  and the LP filters modeling the REF (40) and VCO (41). The equation is rearranged to isolate the offset frequency  $f$ . Then the estimator for the (offset) frequency can be written as

$$\hat{f} = \hat{f}_{3\text{dB}} \sqrt[k]{\left(\frac{1}{10^{\hat{\mathcal{L}}/10\pi\hat{f}_{3\text{dB}}}} - 1\right)}. \quad (50)$$

By inserting  $\hat{f}_{3\text{dB}} = \hat{f}_{3\text{dB,REF}}$  and  $\mathcal{L} = \hat{\mathcal{L}}_{\text{TR}}$ , the transition interval start frequency  $\hat{f}_{\text{TR}}$  is found. In similar fashion, the PLL bandwidth  $\hat{f}_{\text{PLL}}$  and noise floor start frequency  $\hat{f}_{\text{NF}}$  can be calculated.

#### D. Comparing Estimates for Different Devices

The procedure for estimating the system model parameters is repeated for all USRP's in the measured dataset [15]. Parameter estimates are calculated as average between all USRP with identical daughterboard type. Phase noise measurements for both RF chains of the X310 models are considered.

As expected, the parameter estimates displayed in table II relating to REF are identical for both daughterboards. This results from using the same reference (see Fig. 11). The characteristics of the VCO differ slightly for both daughterboards. This can be explained by both daughterboards having different VCO models as described in section V. A significant difference occurs in start frequency of the transition interval and its magnitude. Also the PLL bandwidth for the UBX daughterboard is much larger (177.3 kHz > 26.6 kHz) than that of the CBX daughterboard. This bandwidth is important for characterizing the impulse response of the PLL. However, if the PLL is assumed to be in lock, this parameter is of lower significance. The measured noise floor shows a slight difference between daughterboard models. It is important to note that this measurement does not necessarily reflect the noise floor that the frequency synthesizing circuit can achieve (cf. [16], [17]). The observed noise floor is influenced by the whole RF circuitry and the measurement device used.

In Fig. 17 the phase noise spectrum of the system model is compared to the measurements for both daughterboard

models. The parameters used are those given in Table II. It is Graphically shown that there is the significant difference in the magnitude of the transition interval.

## VII. CONCLUSION

In this paper, a parametric phase noise model for a generic PLL is derived based on existing models from the literature. This derivation is obtained by analyzing the PLL dynamics in the time domain. The phase noise characteristics of common SDR devices, specifically the USRP X310 from National Instruments, are measured. The parameters of the derived phase noise model are fitted to the recorded measurements.

Key findings are the phase noise model parameters listed in Table II for the two examined daughterboards of USRP X310 and estimators for phase noise model parameters from measured phase noise PSD described in section VI. These estimates can be used with discrete phase noise models for free running oscillators and PLL's given in section III and IV to generate phase noise processes in time domain with identical statistical properties to the measured devices. Furthermore, the estimators given in section VI can be used to estimate the phase noise model parameters of any PLL or free running oscillator.

## ACKNOWLEDGMENTS

This work was supported by BMBF under the project KOMSENS-6G (16KISK124) and by the Hexa-X-II project funded from SNS JU under Grant Agreement No 101095759.

## APPENDIX A

### PHASE NOISE IN PHASE-LOCKED LOOPS

Previous works [5] have shown that phase noise analysis leads to a system of differential equations

$$\frac{d}{dt}\mathbf{y} = -\mathbf{A}\mathbf{y} + \mathbf{B}\xi. \quad (51)$$

The vector  $\mathbf{y}(t) = [\beta(t), \gamma(t), \dots]^T$  represents state variables and is of length  $p$ . The order of PLL  $p$  is characterized by the order of LF  $p - 1$ . The noise sources of PLL are represented by the vector  $\xi(t)$  of length  $q$ . With  $q$  representing the number of independent noise sources. The matrices  $\mathbf{A}$ ,  $\mathbf{B}$  are of dimension  $p \times p$  and  $p \times q$  respectively. Using (8) we can rewrite (51)

$$d\mathbf{y}(t) = -\mathbf{A}\mathbf{y}(t)dt + \mathbf{B}d\mathbf{W}(t), \quad (52)$$

where the vector  $d\mathbf{W}(t)$  of length  $q$  represents independent Wiener-processes. This stochastic differential equation is known in the literature [12], [19] as the Langevin equation. Its solution is a OU process [19, p.109, 4.4.43]

$$\mathbf{y}(t) = \mathbf{y}(0)e^{-\mathbf{A}t} + \int_0^t e^{-\mathbf{A}(t-t')} \mathbf{B}d\mathbf{W}(t'). \quad (53)$$

Note that the “starting state” of the OU process  $\mathbf{y}(0)$  is a vector of random variables. Since the starting value is not significant for the statistical properties of the process, it is defined as a deterministic value  $\mathbf{y}(0) \equiv 0$ . Vector  $\mathbf{y}(t)$  consists of a vector of wiener processes  $d\mathbf{W}(t)$ . Its increments are zero

mean, independent, Gaussian-distributed random variables. Therefore, the vector of state variables is also zero mean.

The stochastic time shift at the output of the PFD is

$$\beta(t) = \alpha_{\text{PLL}}(t) - \alpha_{\text{REF}}(t) \quad (54)$$

$$= \alpha_{\text{PLL}}(t) - \sqrt{c_{\text{REF}}} \int_0^t \xi_{\text{REF}}(t') dt'. \quad (55)$$

Note that here the assumption is that the reference oscillator is a free-running oscillator (equivalent to the model established previously), characterized by the oscillator constant  $c_{\text{REF}}$ . The stochastic time shift at the output of the PLL is

$$\alpha_{\text{PLL}}(t) = \sqrt{c_{\text{CTL}}} \int_0^t \gamma(t') dt' + \sqrt{c_{\text{VCO}}} \int_0^t \xi_{\text{VCO}}(t') dt'. \quad (56)$$

Using (55) and (56), the differential in time for the process  $\beta(t)$  can be expressed as

$$\begin{aligned} \frac{d\beta(t)}{dt} &= \sqrt{c_{\text{CTL}}} \gamma(t) + \sqrt{c_{\text{VCO}}} \xi_{\text{VCO}}(t) - \sqrt{c_{\text{REF}}} \xi_{\text{REF}}(t) \\ &= \sqrt{c_{\text{CTL}}} (-k_{\text{PFD}} \beta(t) * h_{\text{LF}}(t)) \\ &\quad + \sqrt{c_{\text{VCO}}} \xi_{\text{VCO}}(t) - \sqrt{c_{\text{REF}}} \xi_{\text{REF}}(t). \end{aligned} \quad (57)$$

## APPENDIX B

### AUTOCORRELATION FUNCTION OF PHASE-LOCKED LOOP OUTPUT PROCESS

In order to find an expression for  $R_{\alpha,\alpha}$ , the ACF  $R_{\beta,\beta}$  and cross-correlation function (CCF)'s  $R_{\alpha,\beta}$ ,  $R_{\beta,\alpha}$  have to be identified. The ACF for the OU-process  $\beta(t)$  is found as

$$R_{\beta,\beta}(t, t + \tau) = \sum_{i=1}^p \nu_i \sum_{j=1}^p \left( e^{-\lambda_i |\tau|} - e^{-(\lambda_i t + \lambda_j (t + \tau))} \right). \quad (58)$$

The variables  $\lambda_i$ ,  $\lambda_j$ ,  $\nu_i$  are introduced in [5]. In the considered configuration of the PLL they are given as

$$\lambda_i = \lambda_j = \lambda = 2\pi f_{\text{PLL}} \quad (59)$$

$$\nu_i = \nu = \frac{c_{\text{VCO}} + c_{\text{REF}}}{4\pi f_{\text{PLL}}}. \quad (60)$$

The ACF over time becomes asymptotically [5, cf. (11)]

$$\lim_{t \rightarrow \infty} s_{\beta,\beta}(t, t + \tau) = \sum_{i=1}^p \nu_i e^{-\lambda_i |\tau|}. \quad (61)$$

The CCF component can be calculated using (53), (31). The integral is solved and mathematical transformations are applied to find

$$R_{\alpha,\beta}(t, t + \tau) = \sqrt{c_{\text{REF}}} \sum_{i=1}^p \mu_i \left( e^{-\lambda_i |\tau|} - e^{-\lambda_i (t + \tau)} \right), \quad (62)$$

and analogously

$$R_{\beta,\alpha}(t, t + \tau) = \sqrt{c_{\text{REF}}} \sum_{i=1}^p \mu_i (1 - e^{-\lambda_i t}). \quad (63)$$

Using the notation in [5] a constant factor is introduced which in our scenario equates to

$$\mu_i = \mu = -\frac{c_{\text{REF}}}{2\pi f_{\text{PLL}}}. \quad (64)$$

Identical to [5, (10)], the sum of the CCF's asymptotically approaches

$$\lim_{t \rightarrow \infty} [R_{\alpha,\beta} + R_{\beta,\alpha}] = \sum_{i=1}^p \mu_i (e^{-\lambda_i |\tau|} + 1). \quad (65)$$

Finally the ACF of  $\alpha_{\text{PLL}}$  at the PLL output can be expressed as

$$\begin{aligned} R_{\alpha,\alpha}(t, t + \tau) &= \sum_{i=1}^p \nu_i \sum_{j=1}^p \left[ e^{-\lambda_i |\tau|} - e^{-(\lambda_i t + \lambda_j (t + \tau))} \right] \\ &\quad + \sum_{i=1}^p \mu_i \left[ e^{-\lambda_i |\tau|} - e^{-\lambda_i (t + \tau)} + 1 - e^{-\lambda_i t} \right] \\ &\quad + c_{\text{REF}} t. \end{aligned} \quad (66)$$

## APPENDIX C

### POWER SPECTRUM DENSITY OF PHASE-LOCKED LOOP

Equivalent to (16) an expression that includes a difference term  $\Delta\alpha = \alpha_{\text{PLL}}(t) - \alpha_{\text{PLL}}(t + \tau)$  and a sum term  $\Sigma\alpha = \alpha_{\text{PLL}}(t) + \alpha_{\text{PLL}}(t + \tau)$  can be obtained. The terms of the expectation of difference and sum are again replaced by their characteristic functions  $\Psi_{\Delta\alpha}$ ,  $\Psi_{\Sigma\alpha}$  (cf. (17), (18)). Similar to (19), (20) the variance for the difference and sum processes has to be calculated. With (34) the variance for the difference process can be written as

$$\begin{aligned} \text{Var}(\Delta\alpha) &= \text{Var}(\alpha_{\text{PLL}}(t) - \alpha_{\text{PLL}}(t + \tau)) \\ &= \text{Var}(\alpha_{\text{PLL}}(t)) - 2R_{\alpha,\alpha}(t, t + \tau) + \text{Var}(\alpha_{\text{PLL}}(t + \tau)) \\ &= \sum_{i=1}^p \nu_i \sum_{j=1}^p \left[ 2 - e^{-(\lambda_i + \lambda_j)t} - e^{-(\lambda_i + \lambda_j)(t + \tau)} - 2e^{-\lambda_i |\tau|} \right. \\ &\quad \left. + 2e^{-(\lambda_i t + \lambda_j (t + \tau))} \right] + 2 \sum_{i=1}^p \mu_i \left[ 1 - e^{-\lambda_i |\tau|} \right] + c_{\text{REF}} |\tau|. \end{aligned} \quad (67)$$

Asymptotically over time the variance for  $\Delta\alpha$  becomes

$$\lim_{t \rightarrow \infty} \text{Var}(\Delta\alpha) = 2 \sum_{i=1}^p (\nu_i + \mu_i) \left[ 1 - e^{-\lambda_i |\tau|} \right] + c_{\text{REF}} |\tau|. \quad (68)$$

In a similar fashion, the variance of the sum process (cf. (20)) is found

$$\begin{aligned} \text{Var}(\Sigma\alpha) &= \text{Var}(\alpha_{\text{PLL}}(t) + \alpha_{\text{PLL}}(t + \tau)) \\ &= \text{Var}(\alpha_{\text{PLL}}(t)) + 2R_{\alpha,\alpha}(t, t + \tau) + \text{Var}(\alpha_{\text{PLL}}(t + \tau)) \\ &= \dots + c_{\text{REF}} (4t + \tau). \end{aligned} \quad (69)$$

Asymptotically over time the variance for  $\Sigma\alpha$  becomes

$$\lim_{t \rightarrow \infty} \text{Var}(\Sigma\alpha) = \infty, \quad (70)$$

and therefore  $\Psi_{\Sigma\alpha} \rightarrow 0$ . Then the asymptotic ACF of the  $\alpha_{\text{PLL}}$  process can be written as

$$\begin{aligned} \lim_{t \rightarrow \infty} R_{x,x}(t, t + \tau) &= \sum_{i=\pm 1} |X_i|^2 e^{ji2\pi f_0 \tau} \Psi_{\Delta\alpha} \\ &+ \underbrace{X_i X_{-i}^* e^{ji2\pi f_0 (2t+\tau)} \Psi_{\Sigma\alpha}}_{=0, \Psi_{\Sigma\alpha} \rightarrow 0} \\ &= \sum_{i=\pm 1} |X_i|^2 e^{ji2\pi f_0 \tau} \\ &\cdot e^{-(2\pi f_0)^2 \left[ \sum_{k=1}^p (\nu_k + \mu_k) [1 - e^{-\lambda_k |\tau|}] + 0.5 c_{\text{REF}} |\tau| \right]}. \end{aligned} \quad (71)$$

In order to make calculating the Fourier transform of the ACF easier, mathematical transformations are applied to receive

$$\begin{aligned} \lim_{t \rightarrow \infty} R_{x,x}(t, t + \tau) &= \sum_{i=\pm 1} |X_i|^2 e^{ji2\pi f_0 \tau} \\ &\cdot \left[ \sum_{n_1=0}^{\infty} \dots \sum_{n_p=0}^{\infty} \left( \eta_{n_k} \cdot e^{-\kappa_{n_k} |\tau|} \right) \right] \end{aligned} \quad (72)$$

The parameters  $\eta_{n_k}, \kappa_{n_k}$  are introduced to allow for more compact notation and represent

$$\eta_{n_k} = e^{-(2\pi f_0)^2 \sum_{k=1}^p (\nu_k + \mu_k)} \prod_{k=1}^p \frac{((2\pi f_0)^2 (\nu_k + \mu_k))^{n_k}}{n_k!} \quad (73)$$

$$\kappa_{n_k} = 0.5(2\pi f_0)^2 c_{\text{REF}} + \sum_{k=1}^p n_k \lambda_k \quad (74)$$

In the specific scenario considered for  $p = 1$  the parameters simplify to

$$\eta_n = \frac{1}{n!} e^{-\frac{\pi f_0^2}{f_{\text{PLL}}} (c_{\text{VCO}} - c_{\text{REF}})} \left( \frac{\pi f_0^2}{f_{\text{PLL}}} (c_{\text{VCO}} - c_{\text{REF}}) \right)^n \quad (75)$$

$$\kappa_n = 2\pi (\pi f_0^2 c_{\text{REF}} + n f_{\text{PLL}}). \quad (76)$$

The PSD of the PLL output is

$$\begin{aligned} S_{x,x}(f) &= \mathfrak{F}_{\tau} \left\{ R_{x,x}(\tau) \right\} \\ &= \sum_{i=\pm 1} |X_i|^2 \delta(f - i f_0) * \left[ \sum_{n=0}^{\infty} \eta_n \frac{2\kappa_n}{\kappa_n^2 + f^2} \right] \\ &= \sum_{i=\pm 1} |X_i|^2 \sum_{n=0}^{\infty} \eta_n \frac{2\kappa_n}{\kappa_n^2 + (f - i f_0)^2}. \end{aligned} \quad (77)$$

## APPENDIX D

### PHASE NOISE MODEL PARAMETERS

Values for the phase noise model parameter estimates for the spectrum displayed in Fig. 15 are given in the following. 3 dB cut-off frequency of REF and VCO

$$\hat{f}_{3\text{dB,REF}} = 0.58 \text{ Hz}, \quad \hat{f}_{3\text{dB,VCO}} = 630 \text{ Hz}.$$

Oscillator constant for REF and VCO

$$\hat{c}_{\text{REF}} = 4.58 \times 10^{-20} \text{ s}, \quad \hat{c}_{\text{VCO}} = 5.01 \times 10^{-17} \text{ s}$$

Transition interval and noise floor power level

$$\hat{\mathcal{L}}_{\text{TR}} = -107.9 \text{ dBc/Hz}, \quad \hat{\mathcal{L}}_{\text{NF}} = -133.7 \text{ dBc/Hz}.$$

Transition interval start frequency, PLL bandwidth and noise floor start frequency

$$\hat{f}_{\text{TR}} = 1865.7 \text{ Hz}, \quad \hat{f}_{\text{PLL}} = 197.9 \text{ kHz}, \quad \hat{f}_{\text{NF}} = 1439.8 \text{ kHz}.$$

Parameter estimates derived from the whole dataset for the two daughterboard types are presented in Table II.

Parameter	CBX
$\hat{f}_{3\text{dB,REF}}$	$0.5570 \pm 0.0249 \text{ Hz}$
$\hat{c}_{\text{REF}}$	$(4.432 \pm 0.1978) \cdot 10^{-20} \text{ s}$
$\hat{f}_{3\text{dB,VCO}}$	$193.4 \pm 16.69 \text{ Hz}$
$\hat{c}_{\text{VCO}}$	$(1.539 \pm 0.1328) \cdot 10^{-17} \text{ s}$
$\hat{\mathcal{L}}_{\text{TR}}$	$-91.9 \pm 1.735 \text{ dBc}$
$\hat{f}_{\text{TR}}$	$538.7 \pm 64.25 \text{ Hz}$
$\hat{f}_{\text{PLL}}$	$26.6 \pm 3.8 \text{ kHz}$
$\hat{\mathcal{L}}_{\text{NF}}$	$-144.4 \pm 0.2197 \text{ dBc}$
$\hat{f}_{\text{NF}}$	$1487 \pm 92.89 \text{ kHz}$
Parameter	UBX
$\hat{f}_{3\text{dB,REF}}$	$0.5853 \pm 0.0503 \text{ Hz}$
$\hat{c}_{\text{REF}}$	$(4.658 \pm 0.4005) \cdot 10^{-20} \text{ s}$
$\hat{f}_{3\text{dB,VCO}}$	$537.6 \pm 63.26 \text{ Hz}$
$\hat{c}_{\text{VCO}}$	$(4.278 \pm 0.5034) \cdot 10^{-17} \text{ s}$
$\hat{\mathcal{L}}_{\text{TR}}$	$-107.8 \pm 0.7843 \text{ dBc}$
$\hat{f}_{\text{TR}}$	$1872.1 \pm 119.61 \text{ Hz}$
$\hat{f}_{\text{PLL}}$	$177.3 \pm 20.04 \text{ kHz}$
$\hat{\mathcal{L}}_{\text{NF}}$	$-134.0 \pm 0.1847 \text{ dBc}$
$\hat{f}_{\text{NF}}$	$1319 \pm 106.20 \text{ MHz}$

TABLE II  
PARAMETER ESTIMATES FOR DIFFERENT DAUGHTERBOARD TYPES GIVEN AS  $\mu \pm \sigma$

## REFERENCES

- [1] C.-X. Wang *et al.*, "On the road to 6G: Visions, requirements, key technologies, and testbeds," *IEEE Commun. Surveys Tuts.*, vol. 25, no. 2, pp. 905–974, 2023.
- [2] F. Bozorgi, P. Sen, A. N. Barreto, and G. Fettweis, "RF front-end challenges for joint communication and radar sensing," in *2021 1st IEEE International Online Symposium on Joint Communications & Sensing (JC&S)*, 2021, pp. 1–6.
- [3] R. W. Heath Jr. and A. Lozano, *Foundations of MIMO Communication*. Cambridge University Press, 2018.
- [4] A. Demir, A. Mehrotra, and J. Roychowdhury, "Phase noise in oscillators: a unifying theory and numerical methods for characterization," *IEEE Transactions on Circuits and Systems I: Fundamental Theory and Applications*, vol. 47, no. 5, pp. 655–674, 2000.
- [5] A. Mehrotra, "Noise analysis of phase-locked loops," *IEEE Transactions on Circuits and Systems I: Fundamental Theory and Applications*, vol. 49, no. 9, pp. 1309–1316, 2002.
- [6] M. Loehning, "Analyse und modellierung der effekte von abtast-jitter in analog-digital-wandlern," Doctoral Dissertation, TU Dresden, Dresden, 2006.
- [7] R. David and D. R. Brown, "Modeling and tracking phase and frequency offsets in low-precision clocks," in *2015 IEEE Aerospace Conference*, 2015, pp. 1–7.
- [8] P. Tschapek, G. Koerner, A. Hofmann, C. Carlowitz, and M. Vossiek, "Phase noise spectral density measurement of broadband frequency-modulated radar signals," *IEEE Transactions on Microwave Theory and Techniques*, vol. 70, no. 4, pp. 2370–2379, 2022.
- [9] 3GPP, "Study on new radio access technology: Radio Frequency (RF) and co-existence aspects," 3rd Generation Partnership Project (3GPP), Technical Report (TR) 38.803, 04 2022, version 14.3.0.

- [10] IEEE, "Ieee standard definitions of physical quantities for fundamental frequency and time metrology—random instabilities," *IEEE Std 1139-2008*, pp. c1–35, 2009.
- [11] D. J. Higham., "An algorithmic introduction to numerical simulation of stochastic differential equations," *SIAM Review*, vol. 43, no. 3, pp. 525–546, 2001.
- [12] A. Papoulis and S. Pillai, *Probability, Random Variables, and Stochastic Processes*, ser. McGraw-Hill series in electrical engineering: Communications and signal processing. Tata McGraw-Hill, 2002.
- [13] D. Petrovic, W. Rave, and G. Fettweis, "Phase noise suppression in ofdm using a kalman filter," 10 2003. [Online]. Available: <https://api.semanticscholar.org/CorpusID:16316446>
- [14] C. Collmann, A. Nimr, and G. Fettweis, "On the impact of phase impairments on angle estimation in true-time-delay systems," in *JC&S 2025*, Oulu, Finland, Jan 2025, p. 6.
- [15] C. Collmann, "Phase Noise Spectrum Dataset for USRP X310," July 2024. [Online]. Available: <https://iee-dataport.org/documents/phase-noise-spectrum-dataset-usrp-x310>
- [16] *Data Sheet: 23.5MHz to 6000MHz Fractional/Integer-N Synthesizer/VCO MAX2870*, Analog Devices, 2017, accessed: 27.05.2024. [Online]. Available: <https://www.analog.com/media/en/technical-documentation/data-sheets/MAX2870.pdf>
- [17] *Data Sheet: 23.5MHz to 6000MHz Fractional/Integer-N Synthesizer/VCO MAX2871*, Analog Devices, 2020, accessed: 27.05.2024. [Online]. Available: <https://www.analog.com/media/en/technical-documentation/data-sheets/MAX2871.pdf>
- [18] S. Xie, "Analyzing and solving fixed frequency spur issues in high precision adc signal chains," *Analog Dialogue*, vol. 51, April 2017.
- [19] C. Gardiner, *Handbook of Stochastic Methods for Physics, Chemistry, and the Natural Sciences*, ser. Proceedings in Life Sciences. Springer-Verlag, 1985.